Chinese Journal of Chemical Engineering 69 (2024) 79–91

Contents lists available at ScienceDirect

Chinese Journal of Chemical Engineering

journal homepage: www.elsevier.com/locate/CJChE

Full Length Article

Molecular simulation study on the evolution process of hydrate residual structures into hydrate

Liwei Cheng [1, 2, 5, *], Yunfei Li [1, 5], Jinlong Cui [2, 3], Huibo Qin [2, 4], Fulong Ning [1, 5], Bei Liu [2, *], Guangjin Chen [2]

[1] Faculty of Engineering, China University of Geosciences, Wuhan 430074, China
[2] State Key Laboratory of Heavy Oil Processing, China University of Petroleum, Beijing 102249, China
[3] College of Science, Nanchang Institute of Technology, Nanchang 330099, China
[4] School of Chemical Engineering, Guangdong University of Petrochemical Technology, Maoming 525000, China
[5] National Center for International Research on Deep Earth Drilling and Resource Development, China University of Geosciences (Wuhan), Wuhan 430074, China

ARTICLE INFO

Article history:
Received 29 September 2023
Received in revised form
26 November 2023
Accepted 17 December 2023
Available online 7 February 2024

Keywords:
Memory effect
Molecular simulation
Hydrate reformation
Residual structures

ABSTRACT

The clathrate hydrate memory effect is a fascinating phenomenon with potential applications in carbon capture, utilization and storage (CCUS), gas separation, and gas storage as it can accelerate the secondary formation of clathrate hydrate. However, the underlying mechanism of this effect remains unclear. To gain a better understanding of the mechanism, we conducted molecular dynamic simulations to simulate the initial formation and reformation processes of methane hydrate. In this work, we showed the evolution process of hydrate residual structures into hydrate cages. The simulation results indicate that the residual structures are closely related to the existence of hydrate memory effect, and the higher the contribution of hydrate dissociated water to the hydrate nucleation process, the faster the hydrate nucleation. After hydrate dissociation, the locally ordered structures still exist after hydrate dissociation and can promote the formation of cluster structures, thus accelerating hydrate nucleation. Additionally, the nucleation process of hydrate and the formation process of clusters are inseparable. The size of clusters composed of cup-cage structures is critical for hydrate nucleation. The residence time at high temperature after hydrate decomposition will affect the strength of the hydrate memory effect. Our simulation results provide microscopic insights into the occurrence of the hydrate memory effect and shed light on the hydrate reformation process at the molecular scale.

1. Introduction

The nonstoichiometric ice-like crystals, called clathrate hydrates, are formed by guest molecules and water molecules at high pressure and low temperature [1]. Gas hydrates were estimated to contain twice as much carbon content as other fossil fuels on earth [2]. On the one hand, gas hydrate is a strategic energy source. Natural gas hydrate has great development value because of its wide distribution, large reserves, high energy density, and high cleanliness [3,4]. The development prospect of natural gas hydrate is highly expected, and gas hydrate has been regarded as an important follow-up energy. Moreover, gas hydrate also have potential applications in carbon dioxide sequestration [5,6], gas storage [7,8], seawater desalination [9], and gas separation [10,11]. On the other hand, hydrate is one of the main culprits of blocking oil and gas pipelines or production equipment, which will cause huge economic losses. The annual economic loss from hydrate plugging exceeds billions of dollars [12]. In recent years, researchers have conducted a lot of research on the commercial development and application of gas hydrates and obtained rich research results [7,13].

The discovery of hydrate dates back to 1810, when Davy [14] accidently discovered that chlorine gas and water can form solids (chlorine gas hydrates) above 273.15 K. The structure of hydrate crystals was not confirmed until the 1950s. According to the difference of crystal structure of hydrate, hydrate can be divided into

* Corresponding authors.
E-mail addresses: chengliwei@cug.edu.cn (L. Cheng), liub@cup.edu.cn (B. Liu).

https://doi.org/10.1016/j.cjche.2023.12.023

sI, sII, and sH [12]. Size of guest molecules will directly affect the type of hydrate formed. Typically, sI hydrate [15] is formed from smaller guest molecules like CH_4, CO_2; sII hydrate [16] is formed from larger guest molecules like C_2H_6, C_3H_4; the guest molecules of sH hydrate [17] are composed of both small and large guest molecules (0.7–0.9 nm). In recent years, a lot of research has been done on the physical properties and thermodynamic properties of gas hydrates [18,19]. A perplexing phenomenon is that the induction time required for hydrate decomposition to reform hydrate is shorter than the induction time required to form hydrate initially [20]. The researchers defined this phenomenon as the hydrate memory effect [21]. As early as 1981, Makogen [22] reported that hydrate dissociated water would form hydrate faster. Subsequently, Parent *et al.* [23] found the thermal history of water can affect the nucleation induction time of methane hydrate. Sefidroodi *et al.* [24] investigated the reformation of cyclopentane hydrate. They found that the memory effect of cyclopentane hydrate was affected by the degree of superheating and time. Giavarini *et al.* [25] found the memory effect can also occur in melt water. Propane hydrate formed faster from melt water than from fresh water. Zhao *et al.* [26] investigated the formation process of sI, sII, and sH hydrate. They noted that the memory effect can occur between different types of hydrate. Obviously, the memory effect can be observed in different types of hydrate reformation. Due to the hydrate memory effect can accelerate the secondary formation of hydrate, the hydrate technology have good application prospects in the fields of gas storage [27] and gas separation [28]. On the other hand, the memory effect can accelerate the blockage of oil and gas production and transportation pipelines, which are problems that plagues the transportation of oil and gas and hydrate exploitation [29]. Therefore, clarifying the essence of the hydrate memory effect is of great significance to the application of hydrate technology and the development of hydrate prevention technology.

Although evidence for the hydrate memory effect is very abundant, the mechanism of the hydrate memory effect is still unclear, which limits the application of hydrate technology and the development of hydrate prevention technology. At present, the most accepted mechanism is the residual structure hypothesis [13]. The residual structure hypothesis holds that the residual hydrate structures remain in the system after hydrate decomposition. When thermodynamic conditions were suitable, hydrate would rapidly reform based on these residual hydrate structures. Sloan *et al.* [20] measured the apparent viscosity of the system after hydrate decomposition and believed that the memory effect was caused by the residual clathrate clusters of water molecules contained in the system after decomposition. Takeya *et al.* [21] pointed out that the hydrate memory effect was due to the metastable polyhedral water molecule clusters wrapped around gas molecules in hydrate dissociation water. Sefidroodi *et al.* [24] found that the memory effect still exists after mixing a small amount of cyclopentane hydrate dissociation water with fresh water. They pointed out that the memory effect may be caused by the presence of residual structures invisible to the naked eye in the liquid phase. Ke *et al.* [30] derived the kinetic model and believed that the residual structure was the main reason for the shortened induction period of hydrate reformation. However, other researchers failed to detect the existence of residual structures when studying the hydrate memory effect by experimental means such as neutron diffraction [31] and Raman spectroscopy [32]. Buchanan *et al.* [33] believed that the residual structure size was too small to be measured by Raman spectroscopy. Due to experimental methods have been unable to detect the existence of residual structures, many researchers have been skeptical of the residual structure hypothesis. Rodger [34] did not detect the ordered water molecule clusters when studying the reformation process of methane hydrate by molecular simulation. They pointed out that the residual methane molecules in the solution after hydrate decomposition were the main cause of the memory effect and proposed the guest supersaturation hypothesis. Subsequently, Zeng *et al.* [35,36] found that the memory effect can be eliminated by antifreeze proteins and proposed the impurity imprinting hypothesis. They believed that the surface of impurity particles would be imprinted after hydrate formation. After the hydrate was decomposed, the surface imprints did not disappear immediately but remain for a period of time and provide memory effect. Recently, Uchida *et al.* [37,38] used transmission electron microscopy to investigate the hydrate formation process. They observed that a large number of long-lived micro-nanobubbles were produced during the dissociation of methane hydrate and ethane hydrate. They reported that these micro-nanobubbles could shorten the hydrate formation and the nanobubble hypothesis was proposed. Cheng *et al.* [39] also found that nanobubbles appeared in the dissociated water after hydrate decomposition, and these bubbles may provide a gas–liquid interface for hydrate reformation. Maeda [40] considered the residual structure to be the least possible hypothesis. He combined the impurity imprinting hypothesis and the nanobubble hypothesis and proposed the interface nanobubble hypothesis. So far, the mechanism of the hydrate memory effect has been controversial, and the physical properties of hydrate memory effect need to be further explored. Li *et al.* [41] believed that the above assumptions were plausible to a certain extent but cannot cover all aspects of observation. The dominant mechanism of memory effects may differ in different systems.

With the development of computer simulation technology, molecular dynamics simulation, as a scientific research method, has become an important means to study the formation process of hydrate [42]. Bai *et al.* [43] used molecular simulation to study the replacement of methane hydrate with carbon dioxide and found that a large number of ring structures remained after the decomposition of methane hydrate. Li *et al.* [44] studied the structural characteristics of molten water by molecular dynamics simulation method. They pointed out that the tetrahedral coordination oxygen atoms were one of the important factors affecting the memory effect. Zheng *et al.* [45] investigated the influencing factors of memory effect by molecular dynamics. They found that the thermal treatment history was important for the memory effect. Therefore, it is highly feasible to use molecular simulation to study the hydrate reformation process, which is conducive to in-depth exploration of the mechanism of memory effect.

Due to the limitations of experimental methods, it is difficult to describe the hydrate reformation process at the microscopic scale. In order to further explore the reformation process of hydrate, the initial formation process and the reformation process of methane hydrate were simulated by molecular dynamics simulation in this work. By analyzing the hydrate nucleation path and the F4 (four-body order parameter) distribution of water molecules, the microscopic process of the initial hydrate formation process and the hydrate reformation process were demonstrated. The evolution process of hydrate residual structures into hydrate was shown during hydrate reformation. By comparing the difference between the initial formation process and the reformation process, we provided microscopic insights into the occurrence of the memory effect of hydrate.

2. Simulation Details

The open-source code for massively parallel simulation software LAMMPS was used for molecular dynamics simulations [46]. The initial size of simulation was set to 5.2 nm × 5.2 nm × 5.2 nm. For the initial configuration of the hydrate-containing system, a

$3 \times 3 \times 4$ unit cell of methane hydrates was placed in the middle of the simulation box as a hydrate layer and 1472 free water molecules were placed in the other regions. The methane hydrate unit cell structure conforms to the Bernal–Fowler ice rule [47]. For the initial configuration of the initial hydrate formation system, 2944 water molecules and 256 methane molecules were randomly distributed in the simulation box.

The TIP4P-ice force field [48] was used to describe the water molecules. The methane molecules were described by single point model. The Lennard–Jones parameters of methane molecules were $\sigma = 0.372$ nm and $\varepsilon = 1.319$ kJ·mol^{-1} [49]. The TIP4P-ice model has been extensively used for water molecules [48,50], and the methane force field has shown its effectiveness in methane hydrate formation [51]. The selection of these force fields was based on existing literature [50,51].The Lorentz–Berthelot combination rule was used to calculate the interaction between different types of atoms. The Lennard–Jones cutoff radius was 1.2 nm. The angles and bond lengths of water molecules were fixed by SHAKE algorithm. The particle-particle particle-mesh (PPPM) summation technique was used to handle the electrostatic interactions. The directions of *x*, *y* and *z* were all set as periodic boundary conditions. For the hydrate decomposition process, the hydrate-containing system was firstly energy-minimized. The canonical ensemble (NVT) simulation at 304 K for 20 ps was performed to relax the solid–liquid interface of hydrate and liquid water molecules and minimize the likelihood of methane hydrate decomposition during the equilibrium phase. Subsequently, the methane hydrate decomposition process was simulated using the constant-pressure, constant-temperature (NPT) ensemble at 304 K and 50 MPa for the hydrate-containing system, thereby obtaining the initial configuration necessary for hydrate reformation. For hydrate initial formation process and reformation process, the systems would be simulated with NPT ensemble at 275 K and 50 MPa. Nosé-Hoover thermostat and pressure barostat were used to maintain temperature and pressure. The time step was set to 1 fs.

3. Results and Discussion

3.1. Methane hydrate decomposition process

Hydrates are ice-like solid formed by water molecules wrapping gas molecules. Water molecules are also known as "hydrate skeletons". In order to explore the reformation of hydrate, we first simulated methane hydrate dissociation process and monitored the number of methane hydrate cages and the total potential energy of the system. Fig. 1(a) showed the schematic diagram of hydrate decomposition at rising temperature. When the temperature rises above the hydrate equilibrium temperature, the hydrogen bond of the hydrate cage would be broken and the guest molecules would escape from the cracked cage. Fig. 1(b) was curves of the number of hydrate cages with time in hydrate decomposition process. When the system was placed in an environment of 304 K and 50 MPa, the system was below the methane hydrate phase equilibrium condition and the methane hydrate would decompose. It can be clearly seen that the number of hydrate cages decreases as the simulation proceeds. The hydrate dissociation process was heterogeneous, and the dissociation rate would increase with the simulation time. The small size of hydrate nuclei was more conducive to hydrate dissociation. This indicated that the smaller the size of the hydrate nucleus was, the more unstable it was. The last methane hydrate cage disappeared at 13.01 ns and the number of methane hydrate cage returned to 0, after which there is no complete hydrate cage structure within the system. This phenomenon indicates that 13.01 ns can be used as the decomposition completion time. Fig. 1(c) were curves of the total potential energy and the number of H-bonds with time in hydrate decomposition process. As the simulation progresses, the number of H-bonds decreases while the total potential energy of the system increases. This occurred due to the decomposition of hydrates and the breaking of hydrogen bonds between water molecules, resulting in a decrease in the system's order. After the completion of hydrate dissociation, the total potential energy and the number of H-bonds of the system did not reach equilibrium. The total potential energy of the system kept increasing, while the number of hydrogen bonds continued to decrease. This occurred because the hydrate cage within the system was disrupted and decomposed, not all five-membered ring or six-membered ring structures formed by water molecules were severed. At 304 K, the five-membered ring or six-membered ring structures gradually weakened, subsequently reducing the level of order among the water molecules. The total potential energy and the number of H-bonds was affected by the further decomposition of the residual damaged hydrate cage structure in the system after hydrate decomposition. Additionally, following the decomposition of hydrates, methane molecules within the system remained in a supersaturated state within the aqueous solution. These methane molecules gradually transitioned out of the liquid phase,

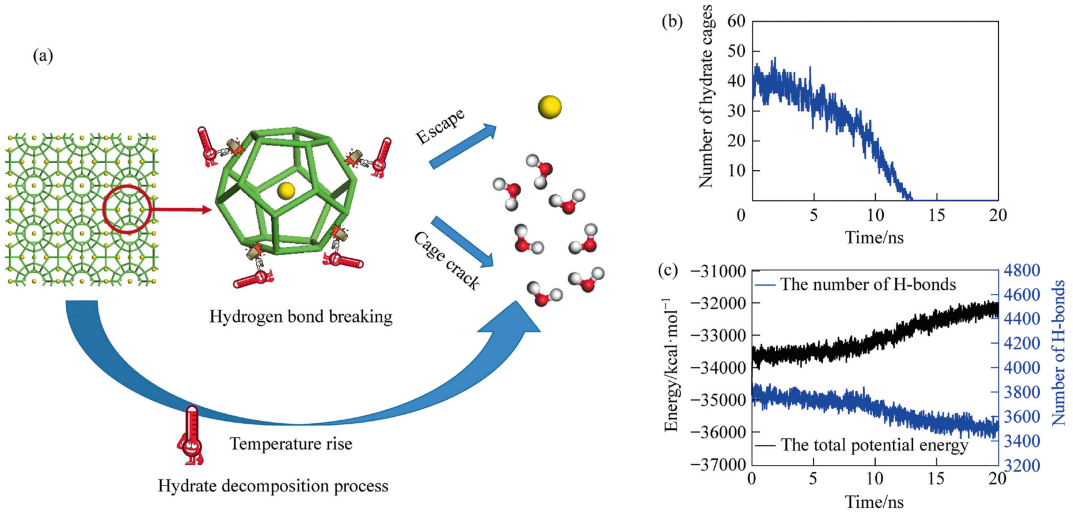

Fig. 1. (a) Schematic diagram of hydrate decomposition process. (b) The variation curve of the number of hydrate cages with time. (c) The variation curve of the total potential energy and the number of H-bonds with time (1 kcal·mol^{-1} = 4.18 kJ·mol^{-1}).

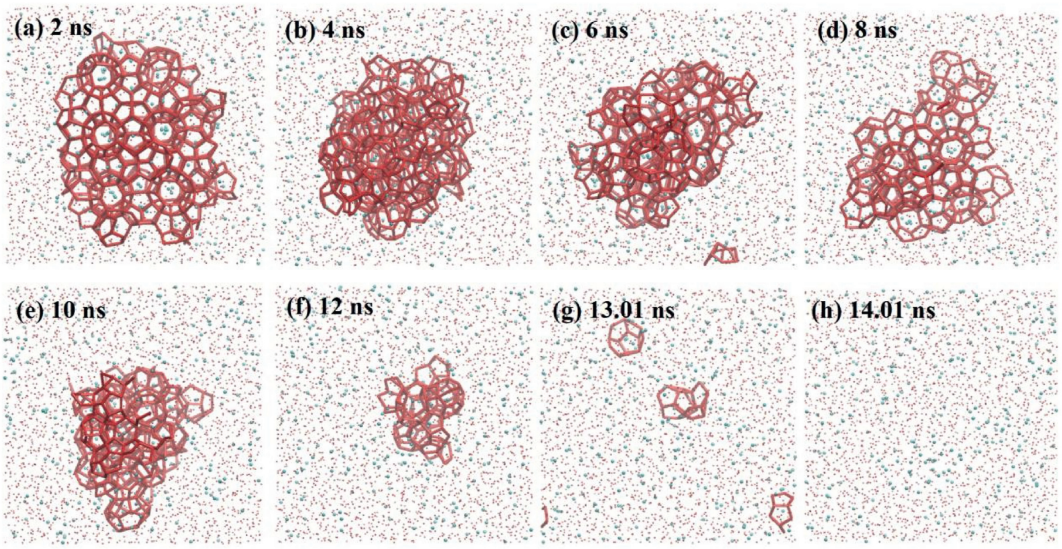

Fig. 2. The trajectory of the methane hydrate decomposition process. The cyan bolls represent methane molecules, the red balls represent water molecules and the red lines represent hydrogen bonds.

aggregating to form methane bubbles, thereby contributing to the reduction in the total potential energy.

Fig. 2 was the trajectory of the methane hydrate decomposition process. At 304 K and 50 MPa, the hydrogen bonds in methane hydrate cages were broken, the hydrate framework collapsed and the methane molecules escaped, resulting in the destruction and decomposition of methane hydrate cage. It can be found from Fig. 2(a)–(f) that the decomposition process preferentially occurs at the solid–liquid interface, where the hydrate surface was in contact with the liquid phase. It was more conducive to the collision of free water molecules with the hydrate cages. The hydrate cages at the solid–liquid interface were more easily disturbed by free water molecules, which led to the hydrogen bonds in the hydrate cage at the solid–liquid interface were more easily broken. The last methane hydrate cage in the system disappeared at 13.01 ns. However, the complete hydrate cage has disappeared and the cup-cage structure after hydrate decomposition still remains in the system. These cup-cage structures were not stable structures. Under the current temperature and pressure conditions, these cup-cage structures would eventually break up and disappear. Obviously, at 14.01 ns, the cup-cage structures were not present in the system.

Fig. 3 showed the F4 order parameter cloud of the methane hydrate decomposition process. The F4 was calculated by the dihedral angle formed by the outermost hydrogen atoms of two adjacent water molecules and the oxygen atoms. The F4 can represent the order of water molecules. The configuration transition of water molecules can be described by the value of F4, which is −0.4 for ice, −0.04 for liquid and 0.7 for hydrates. The initial structure was composed of hydrate and free water, and the F4 value of the hydrate-containing area was significantly higher than that of non-hydrate area. As the hydrate decomposition, the hydrate area was also gradually decreasing. Correspondingly, the F4 of the hydrate-containing area gradually decreased and the order of the system was decreased. This indicated that the water molecules were changing from hydrate to liquid water. The last methane hydrate cage in the system disappeared at 13.01 ns. In Fig. 3(g), the F4 value of local areas in the system was still higher than that in other regions. This is due to the broken hydrate structures remaining in the system after the hydrate cages were destroyed. However, these residual structures were not stable structures and would be gradually decomposed as the simulation proceeds. At 14.01 ns, the F4 value of the last hydrate cage decomposition region was basically the same as that of the other regions. This indicates that the degree of order of the system was further reduced. In the subsequent simulation process, we took the configurations of 13.01 ns and 14.01 ns as the starting point of

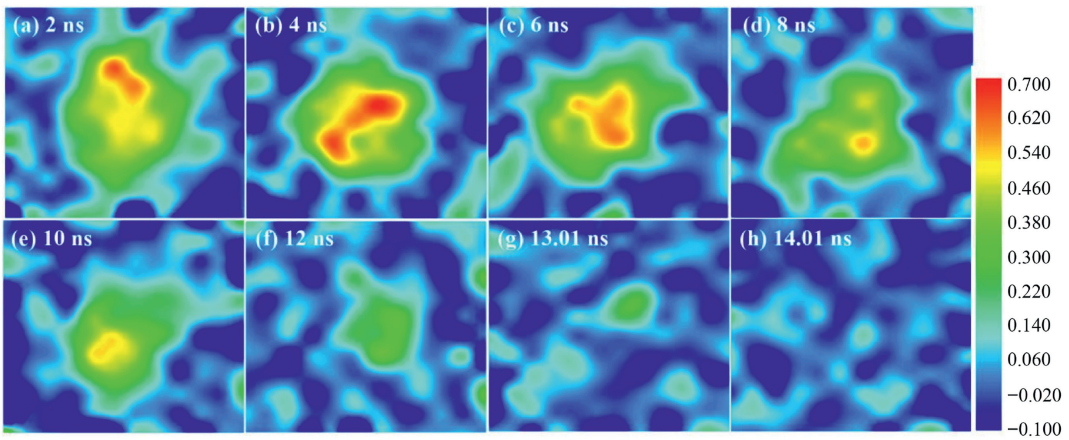

Fig. 3. The F4 order parameter cloud pictures of the decomposition process of methane hydrate.

the hydrate reformation process to explore the microscopic perspective of hydrate reformation.

3.2. Methane hydrate formation and reformation process

In order to compare the difference between the initial formation and reformation of hydrate, we simulated the initial formation process (Run 1) and the reformation process (Run 2 and Run 3) of methane hydrate. For the simulation process of initial formation of hydrate, the initial configuration was composed of 2944 water molecules and 256 methane molecules by randomly distribution. For the simulation of the reformation process of methane hydrate, we simulated two cases. One was to simulate the reformation of hydrate immediately after the completion of hydrate decomposition (Run 2), and the other was to simulate hydrate reformation after 1 ns of hydrate decomposition (Run 3). Decomposition process trajectories of methane hydrate at 13.01 ns (Fig. 2(g)) and 14.01 ns (Fig. 2(f)) were the initial configurations of Run 2 and Run 3, respectively. All hydrate formation processes were carried out at 275 K and 50 MPa. The driving force of hydrate formation can be increased and the simulation time can be shortened by setting the simulation condition as high supercooling condition. It's important to highlight that all of our simulations of the hydrate formation process were carried out under relatively high subcooling conditions, approximately 24.38 K, using methane supersaturated solution. This approach was adopted to reduce the simulation time required for hydrate nucleation. The initial structures of different systems were shown in Fig. 4.

Fig. 5 showed the variation curve of the number of hydrate cages during the hydrate formation process and the reformation process. For the initial hydrate formation system of Run 1, we can found that the first complete hydrate cage formation time was 4.8 ns. But this hydrate cage cannot be served as hydrate nucleation site to support hydrate growth, and the number of cages would soon return to zero. Before the formation of stable hydrate cages, metastable hydrate cages had preferentially appeared in the Run 1 system. Frequent formation and decomposition of metastable hydrate cages changed the local order of the water molecule, which was beneficial to the formation of stable hydrate cages. A stable hydrate cage was formed in the Run 1 system at about 16.40 ns. After that, more methane hydrate cages started to form. This result was consistent with our previous simulation results [50]. For the hydrate reformation system of Run 2, the first metastable hydrate cage formation time was about 0.48 ns and the first stable cage formed at about 3.3 ns. The hydrate nucleation time of Run 2 system was shorter than that of Run 1 system. This phenomenon indicated that there was an obvious hydrate memory effect in the Run 2 system. To verify the reliability of the data, we performed two repeated simulations of the Run 2 system, and the results were depicted in Fig. 5(c). The consistency of the hydrate cage number change curves observed from three repeated simulations of the Run 2 system validated the reliability of our simulation results. For the Run 3 system, the formation time of the first metastable hydrate cage was about 3.06 ns, while the metastable hydrate cages were frequently formed and decomposed during 3.06–15.67 ns. The first stable hydrate cage formed at about 15.67 ns, which was significantly longer than that of the Run 2 system. Compared with the Run 2 system, the hydrate memory effect of the Run 3 system was not obvious, and the induction time of hydrate in Run 3 system was similar to that in Run 1 system. This indicates that when the system was kept at 304 K and 50 MPa for 1 ns after the completion of methane hydrate decomposition, the induction time required for methane hydrate reformation was prolonged and the hydrate memory effect was weakened. The residence time at higher temperature after hydrate decomposition would affect the strength of the hydrate memory effect. Our result was consistent with the experimental results [24,52].

Fig. 6 showed the number of 5^{12} cages, $5^{12}6^2$ cages, $5^{12}6^3$ cages and $5^{12}6^4$ cages in different systems. The 5^{12} cage and $5^{12}6^2$ cage are the components of sI type hydrate. The $5^{12}6^3$ cage is an important bridge between sI type hydrate and sII type hydrate, and the 5^{12} cage and $5^{12}6^4$ cage are the components of sII hydrate. The number of hydrate cages in the different systems followed the order of 5^{12} cages > $5^{12}6^2$ cages > $5^{12}6^3$ cages > $5^{12}6^4$ cages. Whether in the initial hydrate formation system or in the hydrate reformation system, the methane hydrate was always dominated by sI hydrate. This phenomenon indicates that methane hydrate reformation does not affect the type of methane hydrate formation preference. However, it can be found that the amount of sII hydrate in the Run 2 system was lower than that in the Run 1 system. The sI methane hydrate has better thermodynamic stability than the sII methane hydrate [53]. The reformation of the methane hydrate in Run 2 system tended to be more thermodynamic stability. This may be due to the fact that the residual structure after hydrate decomposition is the residual structure of sI type hydrate, which makes it easier to reform sI hydrate.

3.3. The mechanism of hydrate memory effect

Due to the existence of hydrogen bonds between water molecules, a large number of hydrogen bond networks would be formed between water molecules. The pentagonal and hexagonal rings formed by the hydrogen network were also the key to form the hydrate cage structure. The simulation results of Bai *et al.* [43] also show that pentagonal and hexagonal rings play an important role in the formation of methane hydrate. However, liquid water, hydrate and ice all contain pentagonal rings or hexagonal rings, which made up of water molecules and hydrogen bonds. Especially, during the induction period of hydrate nucleation, the number of pentagonal and hexagonal rings does not show obvious characteristics. In addition, pentagonal and hexagonal rings in liquid water were very unstable and easy to decompose, which was not conducive to the monitoring of

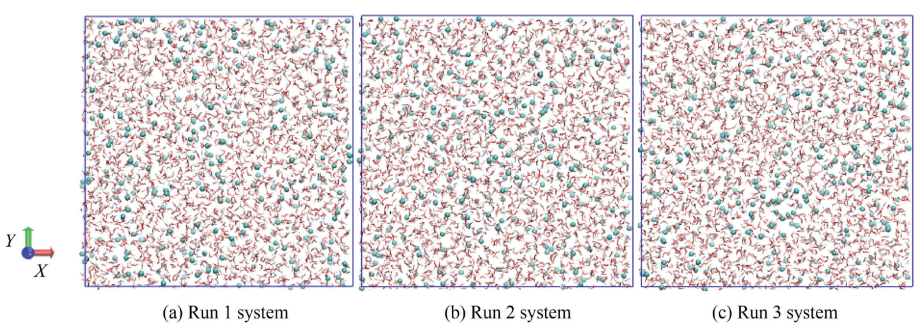

Fig. 4. The initial structure of different systems (the methane molecules were represented by cyan ball models, the water molecules were represented by line model, with oxygen atoms shown in red and hydrogen atoms shown in white).

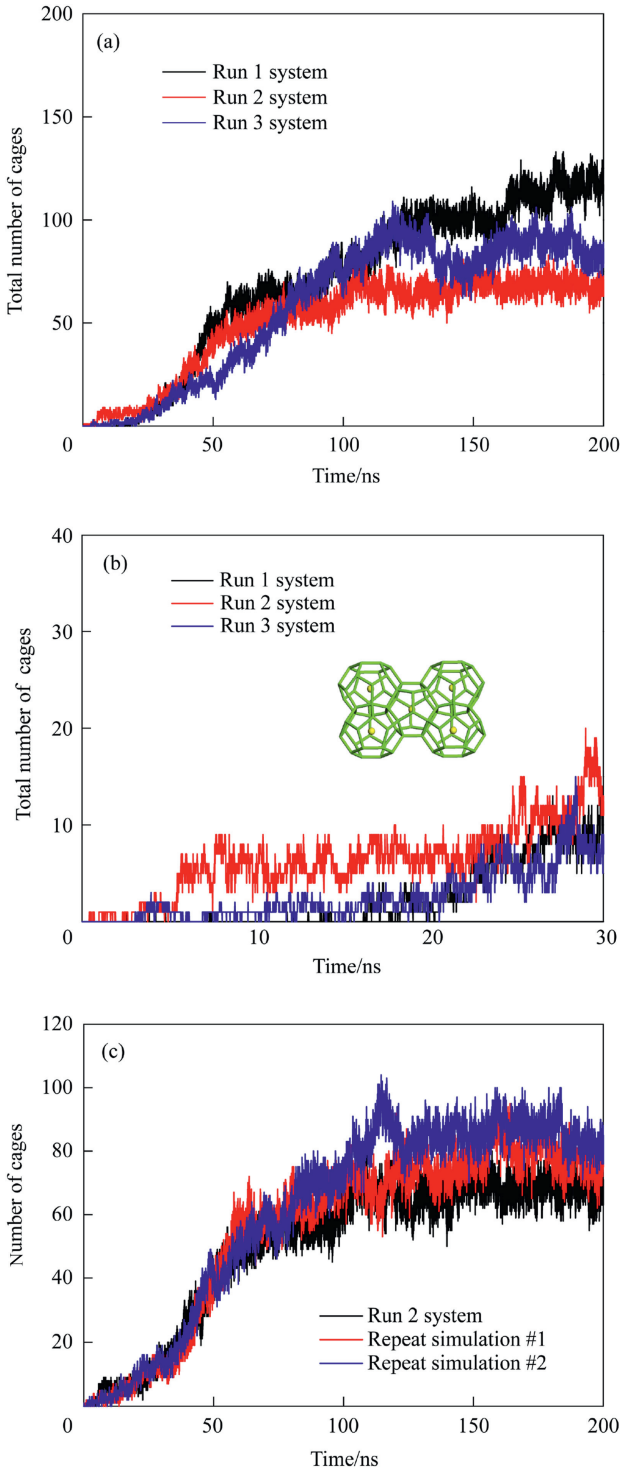

Fig. 5. (a) Variation curves of hydrate cage counts over time in different systems; (b) cage count variation curves from 0 to 30 ns; (c) repeat simulations of the Run 2 system.

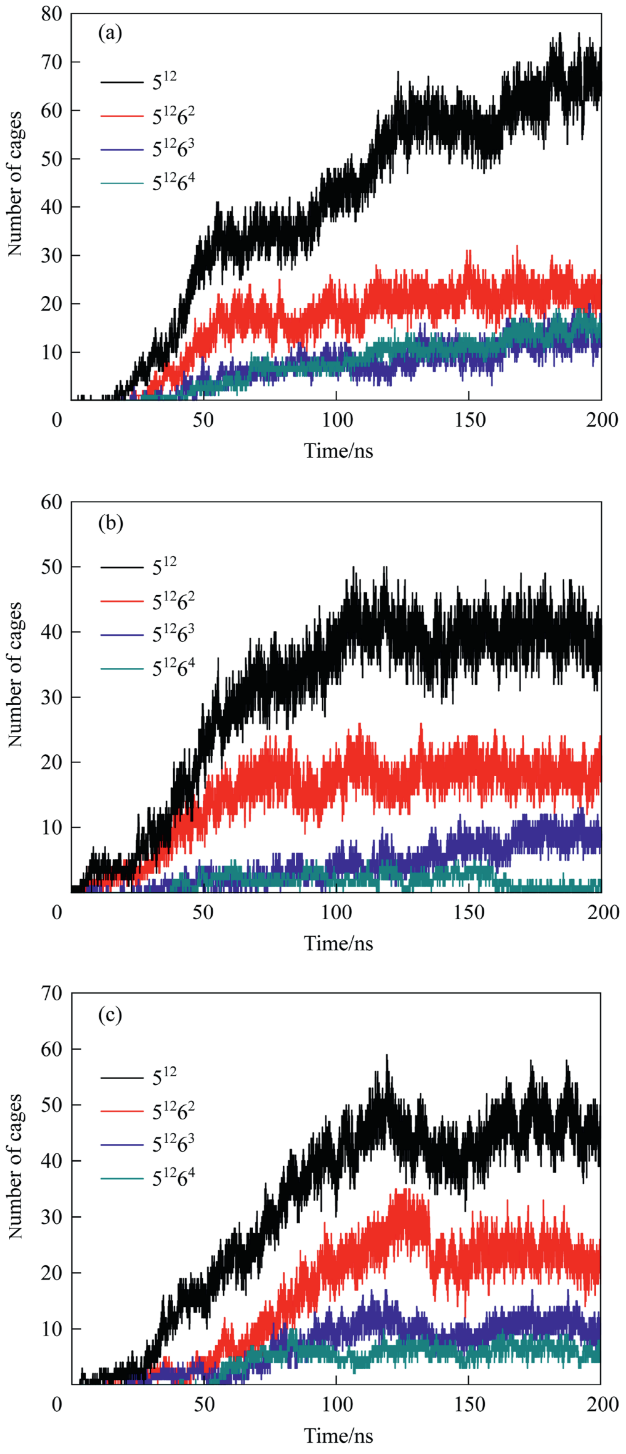

Fig. 6. The number of 5^{12} cages, $5^{12}6^2$ cages, $5^{12}6^3$ cages, and $5^{12}6^4$ cages in (a) Run 1 system, (b) Run 2 system and (c) Run 3 system.

the hydrate nucleation process. In this work, we focused on monitoring the cup-cage structures on the hydrate nucleation process. The cup-cage structure consists of multiple pentagonal or hexagonal rings, which have better stability than individual pentagonal or hexagonal rings. And cup-cage structures are important precursors for the formation of complete hydrate cages, which is of great significance for studying the hydrate formation and reformation process.

Fig. 7 was the hydrate nucleation trajectory of the Run 1 system. It was obvious that the cup-cage structure was preferentially formed before the hydrate nucleation. As showed in Fig. 7(b), the cup-cage structures formed by the splicing of pentagon rings or hexagon rings were randomly distributed in the system. Initially, cup-cage structures formed in the system were very dispersed. The cup-cage structures were unstable structures, which often form and decompose during the simulation. In Fig. 7(c), the system formed the first independent complete hydrate cage at 4.8 ns. However, this independent complete hydrate cage cannot serve as nucleation sites for hydrate growth, which was easily destroyed by collisions of surrounding water and methane molecules. As the

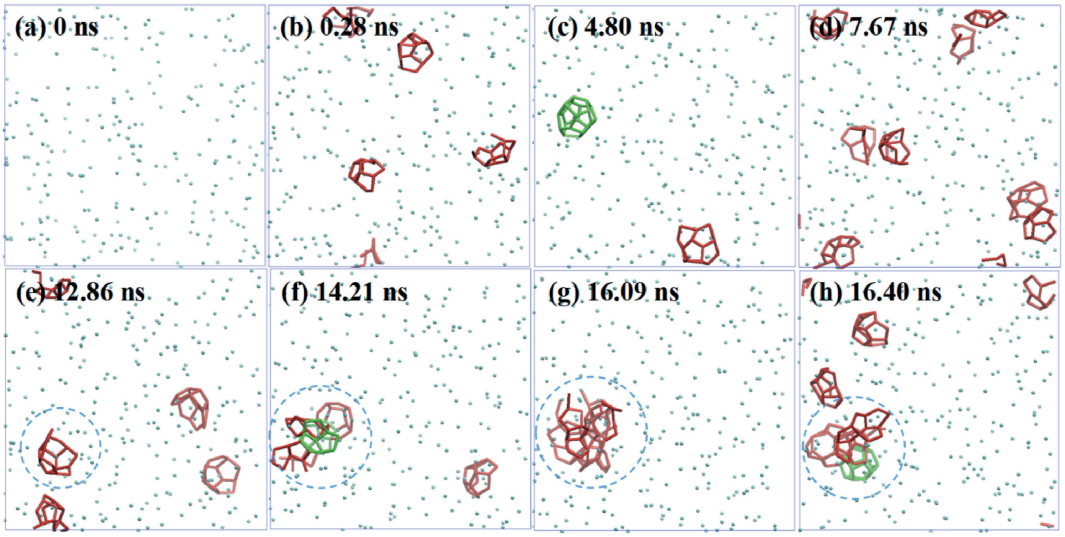

Fig. 7. The hydrate nucleation trajectory of the Run 1 system (the cyan bolls represent methane molecules, cup-cage structures are in red and complete hydrate cages are in green).

simulation progressed, more cup-cage structures formed in the system. Starting from 12.86 ns, the cup-cage structures always appeared in the lower left part of the simulation box. Since the cup-cage structure provided support for the surrounding water and methane molecules, more cup-cage structures were formed around it. As showed in Fig. 7(f)–(g), several cup-cage structures were combined to form cluster structures, and the formation of cluster structures could increase the stability of the cup-cage structures. However, cluster structures were also metastable structure that frequently form and decompose during the simulation process. Finally, the stable hydrate cage was formed at 16.4 ns. From the trajectory snapshots, it can be found that the nucleation process of hydrate and the formation process of clusters were inseparable. Large-sized clusters must form before the stable hydrate nuclei appeared, which was consistent with our previous results [42]. The key to the formation of stable hydrate cage was not the number of cup-cage structures, but the size of the cluster structures composed of cup-cage structures.

Figs. 8 and 9 was snapshots of the hydrate reformation process for the Run 2 and Run 3 systems. For the Run 2 system, it was manifestly seen that there were residual cup-cage structures in the system after the hydrate decomposition. These residual cup-cage structures were significantly smaller than the critical nucleus size [54,55]. The cup-cage structures were fragment of hydrate cages. As showed in Fig. 8(a)–(c), these residual hydrate cup-cage structures were still metastable structures, which would continue to decompose and reform as the simulation progresses. The new cup-cage structures were more likely to form around the residual cup-cage structure, which made it easier to form the cluster structure in Run 2 system. This is due to the relatively high order degree of water molecules in this region after hydrate decomposition. The residual structure can provide skeleton support for surrounding water and methane molecules, which was conducive to the formation of new cup-cage structures. On this basis, the cluster structures composed of several cup-cage structures would be formed rapidly, and the cluster structure was the key of hydrate nucleation. As showed in Fig. 8(c), the Run 2 system formed the first metastable hydrate cage at 0.43 ns. Obviously, the formation of metastable hydrate cage in the Run 2 system was earlier than that in the Run 1 system due to the existence of residual structure. When the cluster structures grow to a certain size, stable hydrate crystal nuclei would be formed in the system. The Run 2 system formed stable hydrate

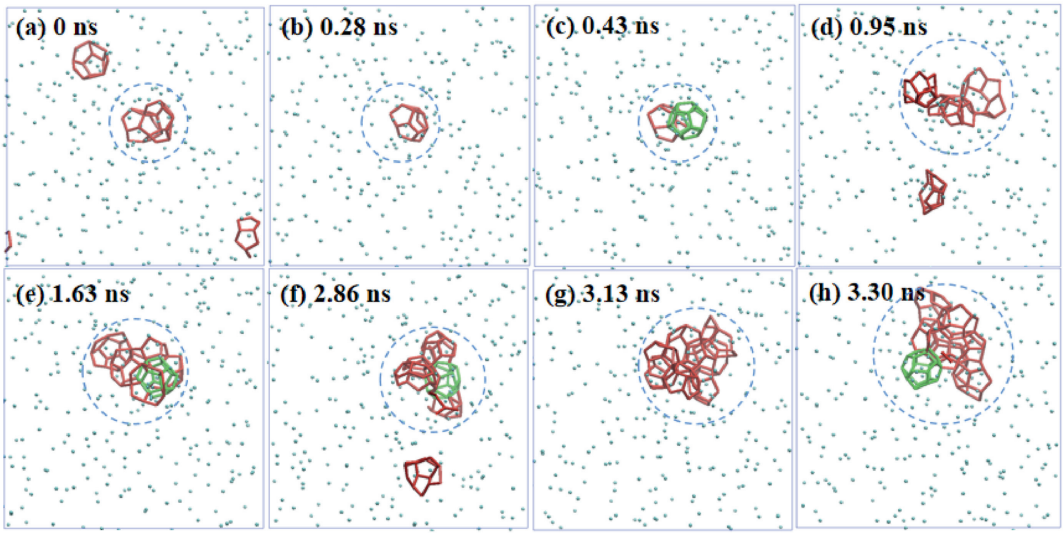

Fig. 8. The snapshots of the hydrate reformation process for the Run 2 systems (the cyan bolls represent methane molecules, cup-cage structures are in red and complete hydrate cages are in green).

nuclei at 3.3 ns. This indicated that Run 2 system had a significant hydrate memory effect. Although the newly formed hydrate cage was not directly formed from the original residual cup-cage structures, the residual cup-cage structures can promote the formation of cluster structures and accelerate the nucleation process of hydrate. The reformation of hydrates takes place near the location where the last fragment of the initial hydrate dissociated. This phenomenon was consistent with the experimental observations described by Oshima *et al.* [32].

Fig. 9 showed snapshots of the hydrate reformation process for the Run 3 system. It can be established from Fig. 9(a) that there was no residual hydrate cup-cage structure in the Run 3 system after the hydrate was decomposed at 304 K and 50 MPa and allowed to stand for 1 ns. During the simulation, the Run 3 system appeared similar to the initial nucleation system, that is, cup-cage structures randomly formed in different regions. Without the support from the residual structures, it would be more difficult for randomly distributed cup-cage structures to form cluster structures. However, the formation of cluster structures was a prerequisite for the hydrate nucleation. The cluster structure formed by cup-cages in the Run 2 system appeared later than that in the Run 1 system. The stable hydrate clusters finally formed stable hydrate cage at 15.67 ns. This phenomenon shows that the hydrate memory effect in the Run 3 system was significantly weakened. The residual cup-cage structures were important for accelerating hydrate reformation. The simulation results show that the residence time after hydrate decomposition can affect the time required for hydrate reformation. The decomposition of the residual cup-cage structures leads to the weakening of the hydrate memory effect and the prolongation of hydrate formation time.

The cup-cage structure serves as a crucial precursor in hydrate cage formation. To further investigate the role of the cup-cage count in hydrate nucleation, Fig. 10 displayed variation curves of the number of cup-cages over time during 0–50 ns for different systems. Throughout the nucleation and growth phases of hydrate formation, the count of cup-cages continued to rise, demonstrating a close association with hydrate formation. At 0 ns, the Run 2 system was the only one showing a non-zero count of cup-cages, and it experienced the most notable growth in this regard. Trajectory analysis from Fig. 8 unveiled a highly concentrated formation of cup-cages in the Run 2 system. Consequently, the critical cluster size was rapidly achieved in the Run 2 system, resulting in nucleation at 3.30 ns. For the Run 1 system, Fig. 7 indicated a scattered formation of cup-cages during the evolution process, which had an adverse effect on hydrate nucleation. The count of cup-cages gradually evolved and eventually nucleated at 16.04 ns after reaching the critical size. In the Run 3 system, significant fluctuations in the count of cup-cages were observed during hydrate nucleation. This was mainly due to the dispersed formation of cup-cages within the Run 3 system, which hindered the formation of stable hydrate cages. The cup-cage counts in different systems revealed that at the moment of hydrate nucleation, clusters within the systems contained 7, 9, and 8 cup-cages for Run 1, Run 2, and Run 3, respectively. This suggests that while the secondary formation of hydrates might influence the rate of cup-cage formation, it does not affect the critical cluster size necessary for hydrate nucleation.

Obviously, the formation of cluster structure was a necessary condition for hydrate nucleation, and the formation of large-scale cluster structure was the key to the formation of stable hydrate cage. As a component of the cluster structure, the evolution process of the cup-cage structure was very important for the hydrate nucleation process. Although the Run 1 and Run 3 systems also formed hydrate cup-cage structures locally at 0.28 ns and 0.22 ns, respectively, the time required for the formation of stable hydrate cage in the Run 1 and Run 3 systems was significantly longer than that of in the Run 2 system. From the trajectory snapshots, it can be found that the cup-cage structures formed early in the Run 1 and Run 3 systems were very dispersed, which made the cluster structure difficult to form. Moreover, some cup-cage structures were deformed, which made these cup-cage structures easy to decompose. We found that the center of the deformed cup-cage structure generally did not contain methane molecules. These deformed cup-cage structures would fail to evolve into complete hydrate cages. The Run 1 and Run 3 systems took longer to form metastable cluster structures. For the Run 2 system, the residual cup-cage structures created excellent conditions for further cluster formation. The residual cup-cage structures can be used as the support point of the new cup-cage structure, and more metastable cup-cage structures were formed around it, so that the cluster structure was easy to form and grow rapidly. The formation and growth rate of the cluster structure was the main factor for the Run 2 system to have a shorter nucleation induction time than the Run 1 and Run 3 systems. Our simulation results show that the residual cup-cage structures are very important for the hydrate memory effect, and these residual cup-cage structures can promote the

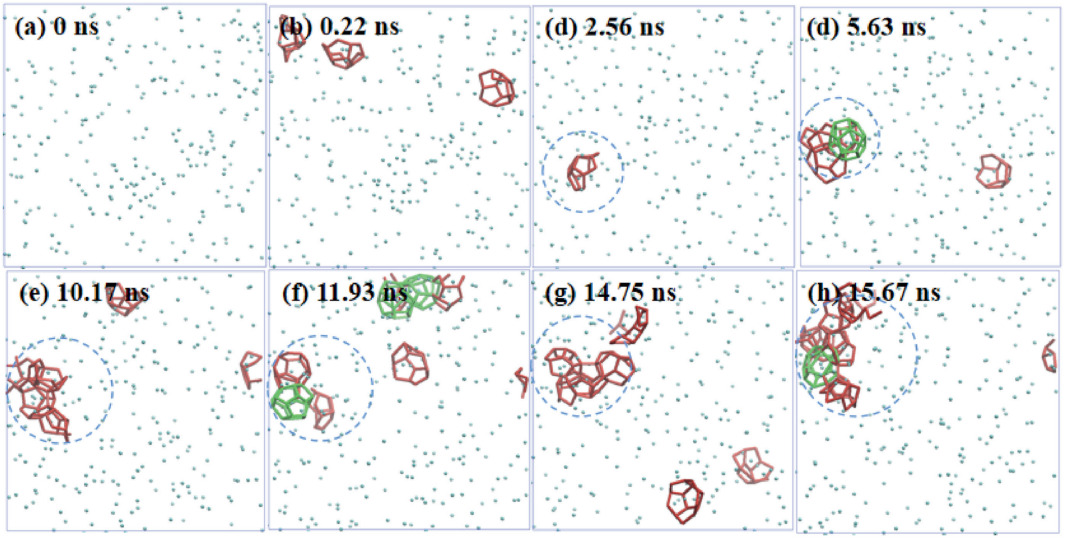

Fig. 9. The snapshots of the hydrate reformation process for the Run 3 system (the cyan bolls represent methane molecules, cup-cage structures are in red and complete hydrate cages are in green).

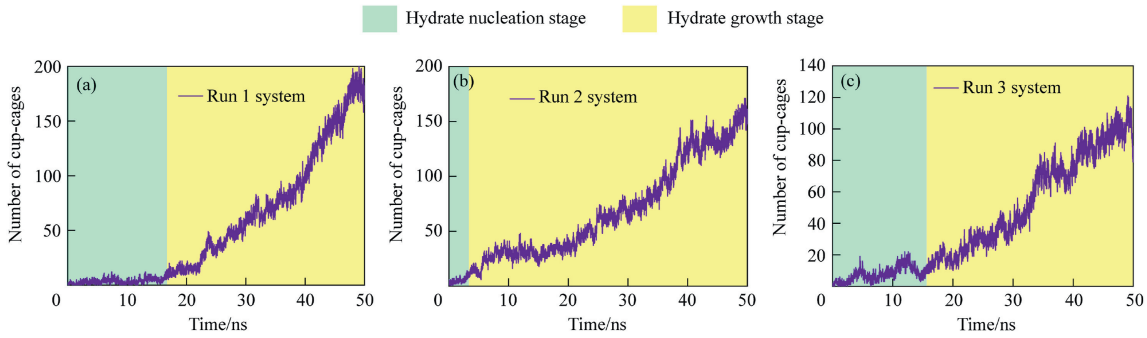

Fig. 10. Variation curves of the number of cup-cages over time during 0–50 ns for different systems.

formation of cluster structures, thereby accelerating hydrate nucleation.

To further clarify the participation of the hydrate dissociated water in hydrate reformation, we marked the water from hydrate dissociation and counted the hydrate dissociated water molecules in the cup-cage structure, cluster structure, and hydrate cage structure. The statistical results were shown in Fig. 11. For the Run 2 system, it can be found that during the hydrate nucleation induction, most of the water molecules forming metastable cup-cage or cluster structures came from the hydrate dissociated water molecules. This indicates that hydrate dissociated water molecules play an important role in hydrate reformation. The higher the contribution of hydrate dissociated water to the hydrate nucleation process, the faster the hydrate nucleation. Obviously, the hydrate memory effect was related to the participation of hydrate dissociated water. When the system entered the growth stage, the participation of hydrate dissociated water dropped to about 0.5. This indicates that the contribution of hydrate dissociated water and free water to hydrate growth was the same. In addition, the simulation condition was set at a higher supercooling and the hydrate growth process was too fast. This made it difficult to explore the effect of the hydrate memory effect on the hydrate growth process. For the Run 3 system, the proportion of hydrate dissociated water involved in nucleation was significantly lower than for the Run 2 system. Correspondingly, the nucleation time of the Run 3 system was longer than that of the Run 2 system. Meanwhile the Run 3 system did not show a significant hydrate memory effect. These simulation results indicated that the existence of hydrate memory effect was closely related to the hydrate dissociated water.

In order to further explore the evolution process of the hydrate cup-cage structures, we analyzed the evolution process of the hydrate cup-cage structures with and without methane molecules, respectively. As showed in Fig. 12(a), the cup-cage structure containing methane molecules evolved from multiple pentagonal ring structures. Methane molecules and a single pentagonal ring were organized to form the precursor of the cup-cage structure. The interaction between the pentagonal ring and methane molecule increased the stability of the pentagonal ring [56]. Methane molecules in hydrates can stabilize pentagonal and hexagonal rings, and the interaction between methane molecules and water molecules plays a certain role in skeleton support. Subsequently, more water molecules formed new pentagonal rings around methane molecules through hydrogen bonds. Finally, the cup-cage structure containing methane molecule was formed. However, the cup-cage structure containing methane molecules was still in a metastable state. During the induction of hydrate nucleation, the cup-cage structures would frequently form and decompose. From Fig. 12(a), it can be found that the cup-cage structure containing methane did not collapse suddenly, but gradually decompose. The formation process and decomposition process of cup-cage structure would take about 0.49 ns and 0.20 ns, respectively. For the cup-cage structure without methane molecule, it can be found that the cup-cage structure did not follow the formation mode of the methane-containing cup-cages. As showed in Fig. 12(b), the hydrogen bond network formed by water molecules directly

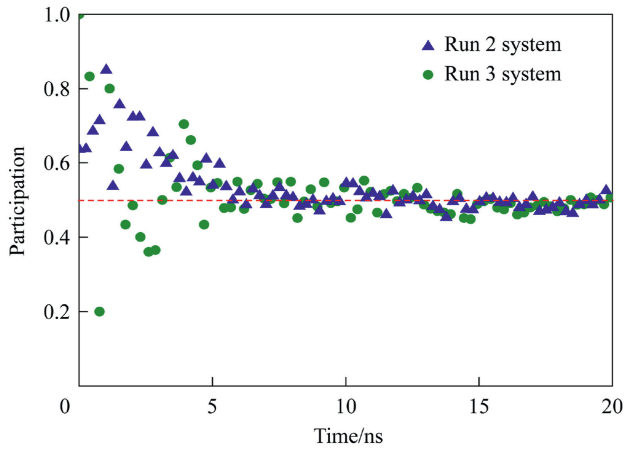

Fig. 11. The participations of hydrate dissociated water in the Run 2 and Run 3 systems.

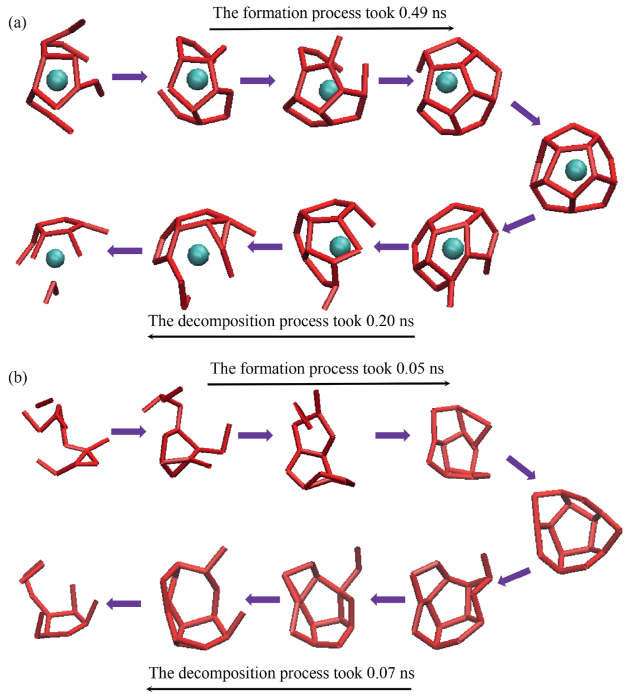

Fig. 12. The evolution processes of the hydrate cup-cage structures (a) with methane molecules and (b) without methane molecules.

formed pentagonal rings. The formation time of the cup-cage structure without methane molecules was faster than that of the cup-cage structure with methane molecules. This indicates that the formation of the cup-cage can be achieved without the participation of methane molecules. However, the cup-cage structure without methane molecule led to the lack of stability of the cup-cage structure, and the decomposition of the cup-cage structure without methane molecule takes only 0.07 ns. The decomposition rate of the cup-cage without methane was faster than that of the cup-cage with methane. This phenomenon further proved that the methane molecules had stabilizing effect on the pentagonal ring structures. The rapid decomposition of the cup-cage structure was not conducive to the increase of the order degree of local water molecules. Therefore, the formation of the cup-cage structure with methane molecule in the system was more conducive to promoting the hydrate nucleation. In the Run 2 system, the residual cup-cage structures contain methane molecules, which can well stabilize the cup-cage structures and make the cup-cage structures have certain stability in the subsequent decomposition and recombination process. This was beneficial for the formation and growth of cluster structures. In contrast, the Run 1 and Run 3 systems need more time to form the cup-cage structure containing methane molecules, which also resulted in the hydrate clusters taking longer time to form. Our simulation results indicated that the hydrate memory effect was linked to the residual structure and methane molecules. The schematic diagram of reformation of hydrate was shown in Fig. 13. The residual structure can provide the skeleton support for the cluster structure and the methane can increase the stability of the hydrate precursor structure. The residual structure containing the cup-cage structures of methane molecules can promote the formation of cluster structures and accelerate the hydrate nucleation.

Figs. 14–16 showed the F4 order parameter cloud for different systems. It can be found that the F4 values in the systems were not uniformly distributed. With the progress of, the local of F4 value and the order degree of water increased. As shown in Figs. 14–16, hydrate nucleation always occurs in regions with higher F4 value.

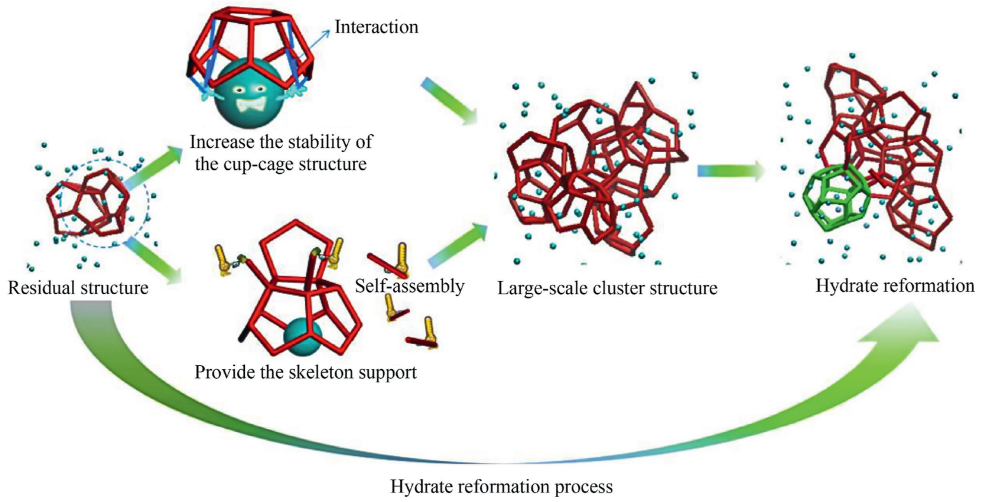

Fig. 13. Schematic diagram of reformation of hydrate.

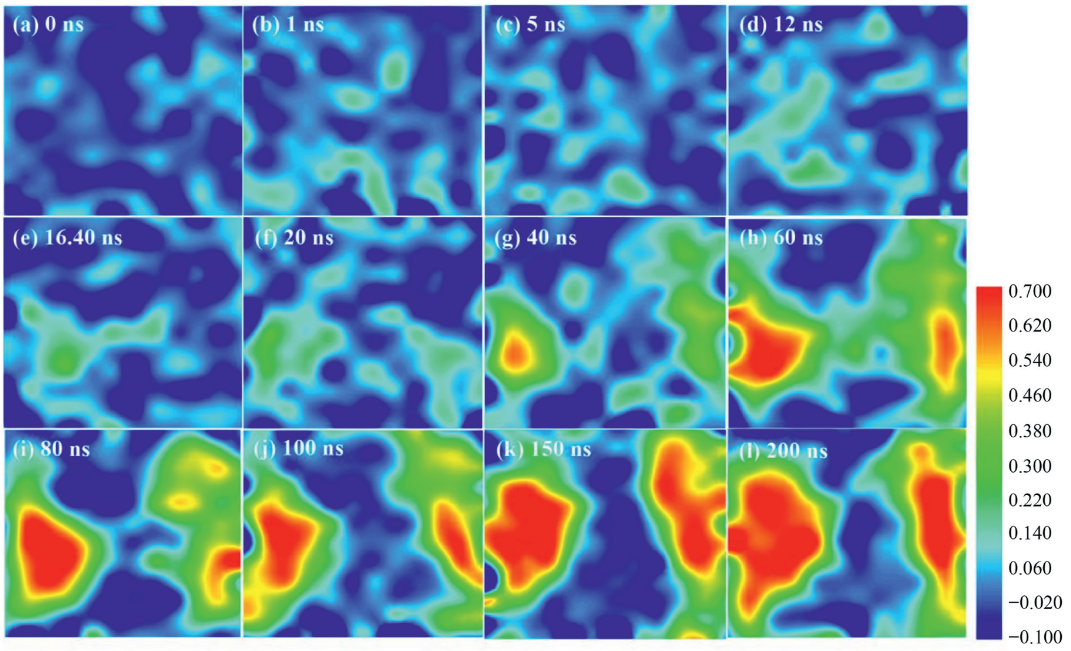

Fig. 14. Evolution of the spatial distribution of F4 for the Run 1 system.

This phenomenon indicates that the high degree of the order of water molecules was necessary for the nucleation of methane hydrate. In our previous discussion, we found that the cluster structures were the key to hydrate nucleation, and stable hydrate cage was evolved from the cluster structures. The formation of the cluster structures was the reason for the increase in the F4 value and order degree of local water molecules. With the formation of hydrates, the F4 value would increase in the hydrate-containing regions of the systems. The state of water molecules can be distinguished by the spatial distribution of the F4 order parameter. It can be clearly seen from Fig. 15(a) that the value of F4 in the area where the last hydrate cage decomposes was still higher than that in other regions. This indicates that the order of water molecules in this region was higher than in other regions. During subsequent simulation, this region acted like a seed and affected the self-assembly of surrounding water molecules. The F4 value around this region increased, and the liquid water molecules were continuously converted into the hydrate. Our simulation results show that the residual high-order water molecule was beneficial to induce the surrounding water molecules to form highly order structure and promote the reformation of methane hydrate. For the Run 1 and Run 3 systems, since there was no obvious high-order water molecule structure in their initial configuration, they would first form local order water molecule structures. This

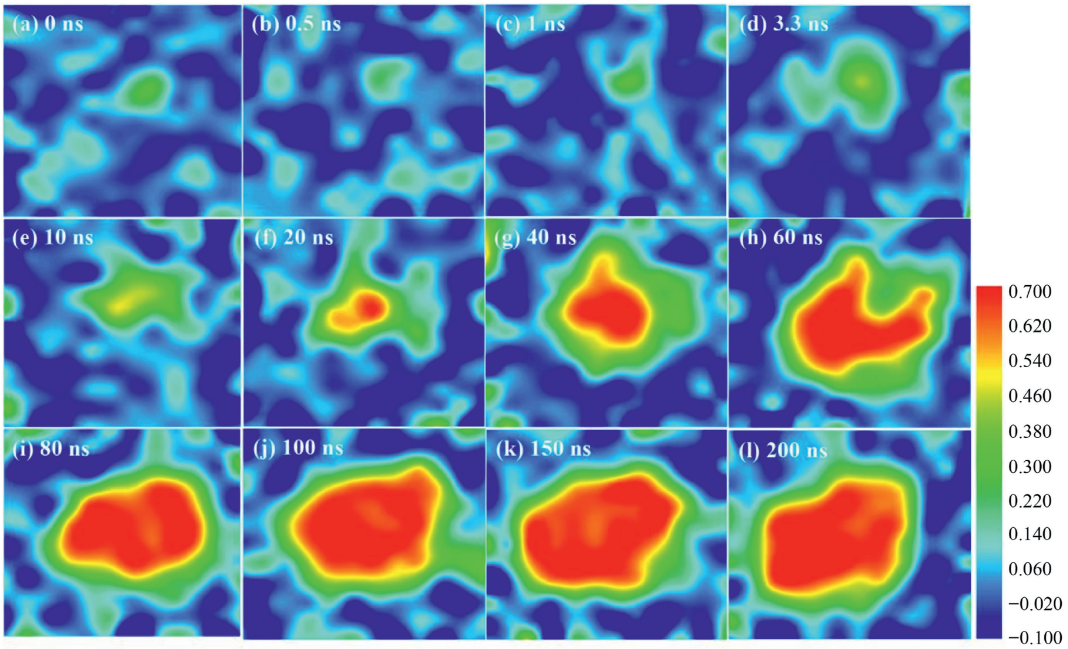

Fig. 15. Evolution of the spatial distribution of F4 for the Run 2 system.

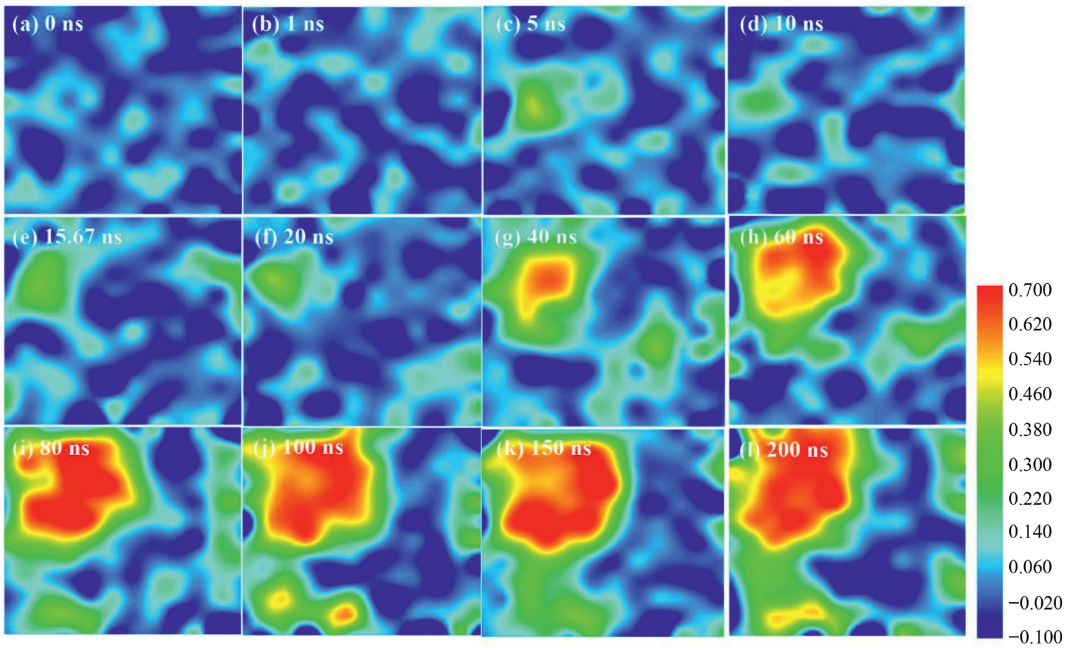

Fig. 16. Evolution of the spatial distribution of F4 for the Run 3 system.

resulted in longer hydrate induction time for the Run 1 and Run 3 systems.

4. Conclusions

The hydrate memory effect, as a perplexing phenomenon, can accelerate the secondary formation of hydrate. To have a better understanding of the mechanism of hydrate memory effect, we simulated the initial formation process of hydrate (Run 1) and the reformation process of hydrate (Run 2 and Run 3). The simulation results show that the nucleation time for the Run 2 system was significantly shorter than that for the Run 1 system. There is obvious hydrate memory effect existing in the Run 2 system. By analyzing the difference between the initial formation process and reformation process, we found that the hydrate memory effect was related to the residual structure and methane molecules. The residual cup-cage structures with methane molecules are critical for the hydrate memory effect, and these residual cup-cage structures can promote the formation of cluster structures, thereby accelerating hydrate nucleation. It can be found that the nucleation process of hydrate and the formation process of cluster structures are inseparable. Additionally, the key to the nucleation of hydrate was not the number of cup-cage structures, but the size of the clusters composed of cup-cage structures. The residence time at high temperature and low pressure after hydrate decomposition would affect the strength of the hydrate memory effect. Our simulation demonstrates the microscopic process of the hydrate reformation process, and provides microscopic insights into the occurrence of the memory effect.

CRediT Authorship Contribution Statement

Liwei Cheng: Methodology, Investigation, Conceptualization, Formal analysis, Writing—original draft. **Yunfei Li:** Methodology, Investigation, Visualization. **Jinlong Cui:** Investigation, Writing—review and editing. **Huibo Qin:** Investigation. **Fulong Ning:** Supervision, Resources. **Bei Liu:** Project administration, Supervision. **Guangjin Chen:** Supervision, Resources.

Data Availability

All data that support the findings of this study are included in this manuscript.

Declaration of Interest

The authors declare that they have no known competing financial interests or personal relationships that could have appeared to influence the work reported in this paper.

Acknowledgements

Financial support from the National Natural Science Foundation of China (22208329, 22178378, 22127812, 21908116 and U19B2005) and Jiangxi Provincial Natural Science Foundation of China (20232BAB213044) are gratefully acknowledged.

References

[1] E.D. Sloan Jr., C.A. Koh, C.A. Koh, Clathrate Hydrates of Natural Gases, CRC Press, Boca Raton, 2007.
[2] N.N. Nguyen, A.V. Nguyen, The dual effect of sodium halides on the formation of methane gas hydrate, *Fuel* 156 (2015) 87–95.
[3] Y.L. Li, N.Y. Wu, D.L. Gao, Q. Chen, C.L. Liu, D.Y. Yang, Y.R. Jin, F.L. Ning, M.J. Tan, G.W. Hu, Optimization and analysis of gravel packing parameters in horizontal wells for natural gas hydrate production, *Energy* 219 (2021) 119585.
[4] Y.L. Li, L. Dong, N.Y. Wu, A. Nouri, H.L. Liao, Q. Chen, J.Y. Sun, C.L. Liu, Influences of hydrate layered distribution patterns on triaxial shearing characteristics of hydrate-bearing sediments, *Eng. Geol.* 294 (2021) 106375.
[5] P. Ndlovu, S. Babaee, P. Naidoo, Review on CH_4-CO_2 replacement for CO_2 sequestration and CH_4/CO_2 hydrate formation in porous media, *Fuel* 320 (2022) 123795.
[6] Y.C. Song, S.J. Wang, Z.C. Cheng, M.X. Huang, Y. Zhang, J.N. Zheng, L.L. Jiang, Y. Liu, Dependence of the hydrate-based CO_2 storage process on the hydrate reservoir environment in high-efficiency storage methods, *Chem. Eng. J.* 415 (2021) 128937.
[7] A. Kumar, H.P. Veluswamy, R. Kumar, P. Linga, Direct use of seawater for rapid methane storage *via* clathrate (sII) hydrates, *Appl. Energy* 235 (2019) 21–30.
[8] P. Xiao, B.C. Dong, J. Li, H.L. Zhang, G.J. Chen, C.Y. Sun, X. Huang, An approach to highly efficient filtration of methane hydrate slurry for the continuous hydrate production, *Energy* 259 (2022) 124892.
[9] J. Mok, W. Choi, Y. Seo, Theoretically achievable efficiency of hydrate-based desalination and its significance for evaluating kinetic desalination performance of gaseous hydrate formers, *Desalination* 524 (2022) 115487.
[10] C.G. Xu, W.J. Xie, G.S. Chen, X.X. Yan, J. Cai, Z.Y. Chen, X.S. Li, Study on the influencing factors of gas consumption in hydrate-based CO_2 separation in the presence of CP by Raman analysis, *Energy* 198 (2020) 117316.
[11] G. Xu, C.G. Xu, M. Wang, J. Cai, Z.Y. Chen, X.S. Li, Influence of nickel foam on kinetics and separation efficiency of hydrate-based carbon dioxide separation, *Energy* 231 (2021) 120826.
[12] A. Hassanpouryouzband, E. Joonaki, M. Vasheghani Farahani, S. Takeya, C. Ruppel, J.H. Yang, N.J. English, J.M. Schicks, K. Edlmann, H. Mehrabian, Z.M. Aman, B. Tohidi, Gas hydrates in sustainable chemistry, *Chem. Soc. Rev.* 49 (15) (2020) 5225–5309.
[13] M.T. Chen, Y.L. Li, Y.J. Zhang, M.H. Qi, N.Y. Wu, Recent advances in creep behaviors characterization for hydrate-bearing sediment, *Renew. Sustain. Energy Rev.* 183 (2023) 113434.
[14] H. Davy, The Bakerian Lecture, On some of the combinations of oxymuriatic gas and oxygene, and on the chemical relations of these principles, to inflammable bodies, *Phil. Trans. R. Soc.* 101 (1811) 1–35.
[15] R.K. McMullan, G.A. Jeffrey, Polyhedral clathrate hydrates. IX. Structure of ethylene oxide hydrate, *J. Chem. Phys.* 42 (8) (1965) 2725–2732.
[16] T.C.W. Mak, R.K. McMullan, Polyhedral clathrate hydrates. X. Structure of the double hydrate of tetrahydrofuran and hydrogen sulfide, *J. Chem. Phys.* 42 (8) (1965) 2732–2737.
[17] J.A. Ripmeester, J.S. Tse, C.I. Ratcliffe, B.M. Powell, A new clathrate hydrate structure, *Nature* 325 (1987) 135–136.
[18] J.M. Schicks, Gas hydrates in nature and in the laboratory: Necessary requirements for formation and properties of the resulting hydrate phase, *ChemTexts* 8 (2) (2022) 13.
[19] C.A. Koh, E.D. Sloan, A.K. Sum, D.T. Wu, Fundamentals and applications of gas hydrates, *Annu. Rev. Chem. Biomol. Eng.* 2 (2011) 237–257.
[20] E.D. Sloan, S. Subramanian, P.N. Matthews, J.P. Lederhos, A.A. Khokhar, Quantifying hydrate formation and kinetic inhibition, *Ind. Eng. Chem. Res.* 37 (8) (1998) 3124–3132.
[21] S. Takeya, A. Hori, T. Hondoh, T. Uchida, Freezing-memory effect of water on nucleation of CO_2 hydrate crystals, *J. Phys. Chem. B* 104 (17) (2000) 4164–4168.
[22] Y.F. Makogon, Hydrates of Hydrocarbons, Texas A & M, University, US, 1997.
[23] J.S. Parent, P. Bishnoi, Investigations into the nucleation behaviour of methane gas hydrates, *Chem. Eng. Commun.* 144 (1) (1996) 51–64.
[24] H. Sefidroodi, E. Abrahamsen, M.A. Kelland, Investigation into the strength and source of the memory effect for cyclopentane hydrate, *Chem. Eng. Sci.* 87 (2013) 133–140.
[25] C. Giavarini, F. Maccioni, M.L. Santarelli, Formation kinetics of propane hydrates, *Ind. Eng. Chem. Res.* 42 (7) (2003) 1517–1521.
[26] J.F. Zhao, C.J. Wang, M.J. Yang, W.G. Liu, K. Xu, Y. Liu, Y.C. Song, Existence of a memory effect between hydrates with different structures (I, II, and H), *J. Nat. Gas Sci. Eng.* 26 (2015) 330–335.
[27] H.P. Veluswamy, G. Bhattacharjee, J.X. Liao, P. Linga, Macroscopic kinetic investigations on mixed natural gas hydrate formation for gas storage application, *Energy Fuels* 34 (12) (2020) 15257–15269.
[28] M.J. Yang, H. Zhou, P.F. Wang, Y.C. Song, Effects of additives on continuous hydrate-based flue gas separation, *Appl. Energy* 221 (2018) 374–385.
[29] Y.C. Song, P.F. Wang, L.L. Jiang, Y.C. Zhao, M.J. Yang, Methane hydrate formation/reformation in three experimental modes: A preliminary investigation of blockage prevention during exploitation, *J. Nat. Gas Sci. Eng.* 27 (2015) 1814–1820.
[30] W. Ke, G.J. Chen, D.Y. Chen, Methane–propane hydrate formation and memory effect study with a reaction kinetics model, *Prog. React. Kinet. Mech.* 45 (2020) 146867832090162.
[31] H. Thompson, A.K. Soper, P. Buchanan, N. Aldiwan, J.L. Creek, C.A. Koh, Methane hydrate formation and decomposition: Structural studies *via* neutron diffraction and empirical potential structure refinement, *J. Chem. Phys.* 124 (16) (2006) 164508.
[32] M. Oshima, W. Shimada, S. Hashimoto, A. Tani, K. Ohgaki, Memory effect on semi-clathrate hydrate formation: A case study of tetragonal tetra-*n*-butyl ammonium bromide hydrate, *Chem. Eng. Sci.* 65 (20) (2010) 5442–5446.
[33] P. Buchanan, A.K. Soper, H. Thompson, R.E. Westacott, J.L. Creek, G. Hobson, C. A. Koh, Search for memory effects in methane hydrate: Structure of water before hydrate formation and after hydrate decomposition, *J. Chem. Phys.* 123 (16) (2005) 164507.

[34] P.M. Rodger, Methane hydrate: Melting and memory, *Ann. N. Y. Acad. Sci.* 912 (1) (2000) 474–482.
[35] H. Zeng, L.D. Wilson, V.K. Walker, J.A. Ripmeester, Effect of antifreeze proteins on the nucleation, growth, and the memory effect during tetrahydrofuran clathrate hydrate formation, *J. Am. Chem. Soc.* 128 (9) (2006) 2844–2850.
[36] H. Zeng, I.L. Moudrakovski, J.A. Ripmeester, V.K. Walker, Effect of antifreeze protein on nucleation, growth and memory of gas hydrates, *AIChE J.* 52 (9) (2006) 3304–3309.
[37] T. Uchida, K. Yamazaki, K. Gohara, Generation of micro- and nano-bubbles in water by dissociation of gas hydrates, *Kor. J. Chem. Eng.* 33 (5) (2016) 1749–1755.
[38] T. Uchida, K. Yamazaki, K. Gohara, Gas nanobubbles as nucleation acceleration in the gas-hydrate memory effect, *J. Phys. Chem. C* 120 (47) (2016) 26620–26629.
[39] C.X. Cheng, F. Wang, T. Qi, P.Y. Xu, Q.G. Zhang, Z.P. Zhang, C. He, J. Zhang, J.L. Zheng, J.F. Zhao, H.Q. Zhang, B. Xiao, Depressurization-induced changes in memory effect of hydrate reformation correlated with sediment morphology, *Energy* 217 (2021) 119374.
[40] N. Maeda, Interfacial nanobubbles and the memory effect of natural gas hydrates, *J. Phys. Chem. C* 122 (21) (2018) 11399–11406.
[41] Y.L. Li, N.Y. Wu, C.Q. He, Z.X. Sun, Z.C. Zhang, X.L. Hao, Q. Chen, Q.T. Bu, C.L. Liu, J.Y. Sun, Nucleation probability and memory effect of methane-propane mixed gas hydrate, *Fuel* 291 (2021) 120103.
[42] L.W. Cheng, J.L. Cui, Z. Li, B. Liu, S. Ban, G.J. Chen, Molecular dynamics simulation of the formation of methane hydrates in the presence of KHIs, *Chem. Eng. Sci.* 236 (2021) 116508.
[43] D.S. Bai, X.R. Zhang, G.J. Chen, W.C. Wang, Replacement mechanism of methane hydrate with carbon dioxide from microsecond molecular dynamics simulations, *Energy Environ. Sci.* 5 (5) (2012) 7033–7041.
[44] Q.B. Li, C. Liu, X. Chen, Molecular characteristics of dissociated water with memory effect from methane hydrates, *Int. J. Mod. Phys. B* 28 (10) (2014) 1450062.
[45] X. Zheng, L.W. Cheng, B. Liu, S. Ban, G.J. Chen, A molecular dynamic simulation on the memory effect of methane hydrate, *J. Mol. Liq.* 363 (2022) 119831.
[46] S. Plimpton, Fast parallel algorithms for short-range molecular dynamics, *J. Comput. Phys.* 117 (1) (1995) 1–19.
[47] J.D. Bernal, R.H. Fowler, A theory of water and ionic solution, with particular reference to hydrogen and hydroxyl ions, *J. Chem. Phys.* 1 (8) (1933) 515–548.
[48] J.L. Abascal, E. Sanz, R. García Fernández, C. Vega, A potential model for the study of ices and amorphous water: TIP4P/Ice, *J. Chem. Phys.* 122 (23) (2005) 234511.
[49] S. Calero, D. Dubbeldam, R. Krishna, B. Smit, T.J.H. Vlugt, J.F.M. Denayer, J.A. Martens, T.L.M. Maesen, Understanding the role of sodium during adsorption: A force field for alkanes in sodium-exchanged faujasites, *J. Am. Chem. Soc.* 126 (36) (2004) 11377–11386.
[50] L.W. Cheng, K. Liao, Z. Li, J.L. Cui, B. Liu, F.G. Li, G.J. Chen, C.Y. Sun, The invalidation mechanism of kinetic hydrate inhibitors under high subcooling conditions, *Chem. Eng. Sci.* 207 (2019) 305–316.
[51] L.W. Cheng, Z. Li, J.L. Cui, R. Zhu, J. Li, H.B. Qin, B. Liu, G.J. Chen, F.L. Ning, The synergistic effect between imidazole reagents and kinetic hydrate inhibitors, *J. Mol. Liq.* 376 (2023) 121466.
[52] D.Y. Wu, S.H. Zhang, H.D. Zhang, X.X. Zhang, P.H. Sun, An experimental study on the characteristics of bulk nanobubbles generated by CO_2 hydrate dissociation, *Fuel* 318 (2022) 123640.
[53] M.R. Walsh, C.A. Koh, E.D. Sloan, A.K. Sum, D.T. Wu, Microsecond simulations of spontaneous methane hydrate nucleation and growth, *Science* 326 (5956) (2009) 1095–1098.
[54] L.C. Jacobson, V. Molinero, Can amorphous nuclei grow crystalline clathrates? The size and crystallinity of critical clathrate nuclei, *J. Am. Chem. Soc.* 133 (16) (2011) 6458–6463.
[55] R. Ma, H. Zhong, L.W. Li, J. Zhong, Y.G. Yan, J. Zhang, J.X. Liu, Molecular insights into the effect of a solid surface on the stability of a hydrate nucleus, *J. Phys. Chem. C* 124 (4) (2020) 2664–2671.
[56] J.X. Liu, J. Hou, J.F. Xu, H.Y. Liu, G. Chen, J. Zhang, Formation of clathrate cages of sI methane hydrate revealed by *ab initio* study, *Energy* 120 (2017) 698–704.